J Nanostruct 15(1): 88-107, Winter 2025

RESEARCH PAPER

Synthesis, Characterization, and Biological Evaluation of Nano Schiff Base Metal Complexes: Antibacterial and Anticancer Potential Against Breast Cancer (MCF-7) Cells

Hayder O. Jamel [1]*, Mohammed Shakir Mwaea [2], Duha M. Eidan [1], Makarim A. Mahdi [1] and Layth S. Jasim [1]

[1] *Department of Chemistry, College of Education, University of Al-Qadisiyah, Iraq*

[2] *Ministry of Education, Directorate of Education Wasit, Wasit, Iraq*

ARTICLE INFO

Article History:
Received 10 September 2024
Accepted 28 December 2024
Published 01 January 2025

Keywords:
Antibacterial
Anticancer
Schiff bases

ABSTRACT

The synthesized nano Schiff base ligand, 2-(((1*E*,2*E*)-2-((4-((*E*)-1-((4,5-dimethylthiazol-2-yl)imino)ethyl)phenyl)imino)-1,2-diphenylethylidene) amino)phenol (DMTDP), and its metal complexes were evaluated for their biological activity and structural properties. DMTDP was synthesized in two steps, producing a compound with 79% yield and molecular formula $C_{33}H_{28}N_4OS$. The metal complexes were formed by reacting DMTDP with various metals, such as Pd(II), Cu(II), Ni(II), Zn(II), Ag(I), and Cd(II), yielding colored complexes. The structural analysis was performed using UV-Vis, FTIR, and XRD spectroscopy, revealing octahedral and square-planar geometries for most metal complexes. The biological activity of the synthesized compounds was assessed against Gram-positive Staphylococcus aureus and Gram-negative Escherichia coli. The palladium complex exhibited the highest antibacterial activity, while other complexes displayed moderate effectiveness. Cytotoxicity assays using the MCF-7 breast cancer cell line demonstrated that the palladium complex had significant cytotoxic effects, with an IC50 of 23.4 µg/mL. The complex also displayed selectivity, showing a higher IC50 (67.5 µg/mL) in normal cells, indicating its potential as an anticancer agent. These findings highlight the importance of Schiff base complexes in biomedical applications, suggesting that palladium-based complexes could serve as promising candidates for anticancer treatments.

How to cite this article
Jamel H., mwaea M., Eidan D, Mahdi M. Jasim L. Synthesis, Characterization, and Biological Evaluation of Nano Schiff Base Metal Complexes: Antibacterial and Anticancer Potential Against Breast Cancer (MCF-7) Cells. J Nanostruct, 2025; 15(1):88-107. DOI: 10.22052/JNS.2025.01.009

INTRODUCTION

Schiff bases, named after chemist Hugo Schiff, are versatile chemicals formed by condensation of primary amines with carbonyl compounds like aldehydes or ketones. These chemicals are readily available in labs due to their affordable and simple production [1]. Owing to their diverse functional properties, Schiff bases have garnered significant attention in various scientific fields, particularly in medicinal and biological applications [2]. A wide spectrum of pharmacological characteristics, such as antiviral, antioxidant, antifungal, anticancer,

* *Corresponding Author Email: haider.hassani@qu.edu.iq*

anthelmintic, antibacterial, antimalarial, anti-inflammatory, antiglycation, anti-ulcerogenic, and analgesic potentials, have been demonstrated for Schiff bases [3, 4]. These versatile compounds have proven valuable in the development of novel therapeutic agents, contributing to advancements in the treatment of various diseases and conditions [2]. Copper Schiff base complexes are utilized in the manufacture of printing inks and dyes. Additionally, Schiff bases have broad applications in analytical chemistry, such as the quantitative determination of ions, and in organic chemistry as intermediates for the synthesis of various organic compounds [5, 6]. They also serve as key precursors in cycloaddition reactions, forming cyclic compounds [7]. Schiff base complexes derived from 2-aminothiazole are particularly notable due to their enhanced properties compared to other Schiff base complexes and their extensive applications, especially in the development of anti-cancer drugs [8]. The efficacy of 2-aminothiazole compounds has made them highly relevant in medicinal chemistry, particularly in the treatment of tumors of various sizes [9]. As scientific advancements progress, researchers continue to explore Schiff base complexes with promising anti-cancer activity, keeping pace with the rapid developments in this field [10]. The strong similarity between the coordination chemistry of palladium(II) compounds has supported the exploration of palladium(II) complexes as potential anti-cancer drugs[11]. Palladium (II) complexes with nano ligands containing various donor atoms have been found to exhibit anti-inflammatory, antimicrobial, anticancer, antibacterial, antiviral, and antifungal properties[12, 13]. Six novel compounds were produced in this work using nano Schiff base ligand that was obtained from 4,5-dimethyl-2-aminothiazole. Numerous methods were employed to characterize the compounds, such as nuclear magnetic resonance spectroscopy (1H, 13C-NMR), X-ray diffraction (XRD), scanning electron microscopy (SEM), infrared spectroscopy (FT-IR), ultraviolet-visible spectroscopy (UV-Vis), and molar conductivity tests. The synthesized nano ligand's biological activity was assessed in relation to two distinct bacterial strains: Gram-positive Staphylococcus aureus and Gram-negative Escherichia coli. Furthermore, the palladium complex's anticancer efficacy was evaluated in relation to both malignant and healthy cells.

MATERIALS AND METHODS

Chemicals and materials

Commercially available and utilized without additional purification were the following chemicals: The following products are from Sigma-Aldrich (Germany): 4,5-dimethyl-2-aminothiazole (C5H8N2S), 4-aminoacetophenone (C8H9NO), benzil (C14H10O2) and 2-aminophenol (C6H7NO), cadmium chloride ($CdCl_2$), copper(II) chloride dihydrate ($CuCl_2{\cdot}2H_2O$), dimethyl sulfoxide (C_2H_6SO), dimethylformamide (C_3H_7NO), nickel(II) chloride hexahydrate ($NiCl_2{\cdot}6H_2O$), palladium(II) chloride ($PdCl_2$), silver nitrate ($AgNO_3$), and zinc chloride ($ZnCl_2$). Deionized water was utilized to prepare all solutions, and all reagents utilized were of analytical grade purity.

Instruments

The electronic spectra were measured on a T80-PG double beam (UV-Vis) spectrophotometer in absolute ethanol using a quartz cuvette of 1 cm path length in the 200-800 nm range. FT-IR spectra (KBr disks, 4000400 cm^{-1}) were recorded using a Shimadzu 8400 S-Field emission scanning electron microscopy (FESEM) images obtained on a MIRA3 TESCAN. X-ray diffraction (XRD) measurements were performed using a Bestec Aluminum anode-Germany X-ray diffractometer with (Cu K_α) radiation (λ¼1.5418 Å) in the range of 2Θ (5-80°).

Preparation of (DMTDP)

The DMTDP compound was synthesized in two steps (Fig. 1). The first step included the preparation of compound A, which is *E*)-4-(1-((4,5-dimethylthiazol-2-yl)imino)ethyl)aniline, which was prepared from dissolving (1.28 g) of 4,5-dimethyl-2-aminothiazole in (25 mL) of absolute ethanol and by continuing to stir, add to it (1.35 g) of 4-aminoacetophenone dissolved in (25 mL) of absolute ethanol. The mixture was refluxed for 8 hours, after which the mixture was cooled, and was observed that a precipitate formed, which was filtered and dried, and then recrystallized from absolute ethanol and then the precipitate was collected, giving a product of (73%). The second step, included the preparation of DMTDP compound by dissolving compound (A) in an amount of (2.45 g) in (25 mL) of absolute ethanol, and by continuous stirring, was added to it a solution (2.1 g) of benzil dissolved in (25 mL) of absolute ethanol and (1.1 g) of 2-aminophenol dissolved in (15 mL) of absolute ethanol and 4-5 drops of glacial acetic acid were

added to the mixture. The mixture was refluxed for 8 hours; then, the mixture was cooled, where it was observed that a precipitate formed, which was filtered and dried, and recrystallized from absolute ethanol. The nano ligand (DMTDP) 2-(((1*E*,2*E*)-2-((4-((*E*)-1-((4,5-dimethylthiazol-2-yl)imino)ethyl) phenyl)imino)-1,2 diphenyl ethylidene)amino) phenol was obtained as solid brown yield 79%, m.p (221-220^{0}C). Elemental analysis agrees with the DMTDP compound formula given in Table 1.

General synthesis of metal complexes

The complexes of the nano ligand were synthesized by reacting it with the following metals: Pd(II), Cd(II), Ag(I), Zn(II), Cu(II), and Ni(II). The general procedure followed for the synthesis is as described: A specified amount of the nano ligand, as detailed in Table 2, was dissolved in 10 mL of absolute ethanol. The metal, also dissolved in absolute ethanol, was then added to the nano ligand solution. The mixture was subjected to reflux with continuous stirring for two hours. After the reaction time, the mixture was cooled, and the precipitate was dried and recrystallized from absolute ethanol. This process yielded pure, colored complexes.

Biological Activity of Preparation Compounds

The biological activity of the synthesized nano ligand and its metal complexes was evaluated against two pathogenic bacterial strains: Gram-positive Staphylococcus aureus and Gram-negative Escherichia coli. These bacterial strains were isolated and identified in the laboratory using biochemical and microscopic tests. The bacterial samples were obtained from Al-Diwaniyah Teaching Hospital, as these strains are among the most prevalent pathogenic bacteria. The bacteria were cultured and activated using the agar diffusion method. The synthesized compounds

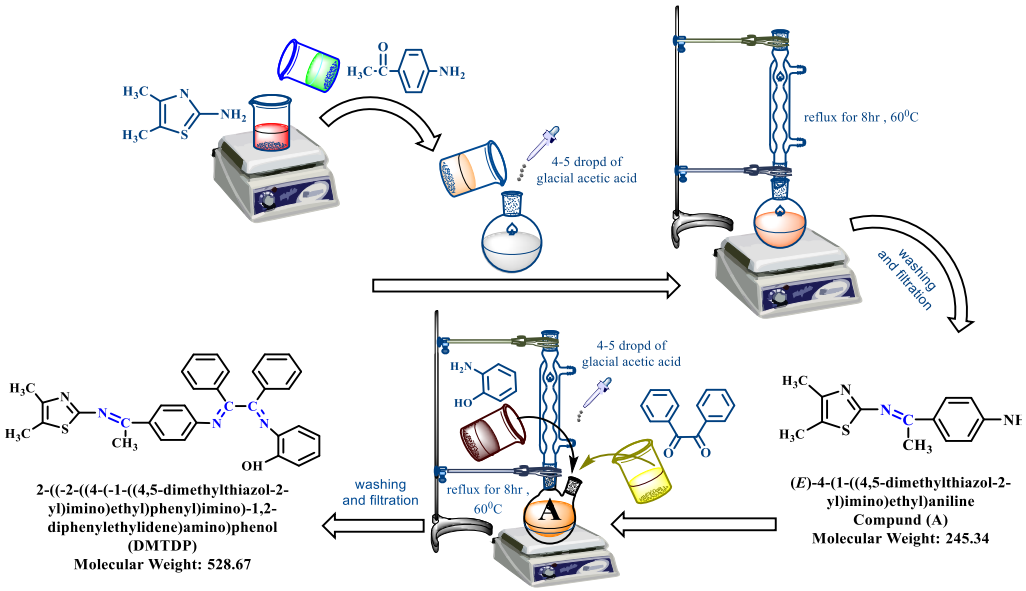

Fig. 1. Preparation of DMTDP compound

Table 1. Elemental analysis and some physical properties of the DMTDP

Compound	Molecular Weight (g/mol)	M.P (°C)	Yield%	Molecular Formula	Found (% Cal.)			
					C	H	N	S
DMTDP	528.67	(221-220)	79	$C_{33}H_{28}N_4OS$	75.35	5.39	10.75	6.11
					74.97	5.34	10.60	6.06

were then tested against these bacterial strains, and the biological activity values for all the compounds were recorded.

Preparation of the nano ligand and its complexes solutions

Solutions for the biological activity tests were prepared at a concentration of 500 ppm. This was achieved by dissolving 0.005 g of either the nano ligand or each metal complex separately in 10 mL of dimethyl sulfoxide (DMSO).

The bacteria were spread on the surface of the Mueller-Hinton agar plates using a loopful. Several wells, each with a diameter of 6 mm, were then created in these plates using a cork borer sterilized with alcohol, ensuring an appropriate distance between the wells to prevent overlapping inhibition zones. The prepared solutions (0.1 mL) were added to the wells using a micropipette. The plates were then incubated for 24 hours at 37°C. After incubation, the diameter of the inhibition zones was measured in millimeters using a ruler. The diameter of each plate was 9 cm.

Cytotoxicity Assays Cell

The MCF-7 breast cancer cell line was cultured using the Freshney technique. The cancer cell line was first defrosted at 37°C in a water bath. Following that, the study's cells were put in a 25 cm^2 animal cell culture flask that was supplemented with 10% foetal bovine serum (FBS) in Dulbecco's Modified Eagle Medium (DMEM). The culture media and cell suspension were placed inside these flasks and incubated for a whole day at 37°C with 5% CO2 in the atmosphere. The cultures were examined following the incubation period to verify the cell line's proliferation. The establishment of secondary cultures helped to avoid contamination. Using an inverted microscope, every cell was inspected to make sure it was viable, free of impurities, and growing to the target cell density of between 500,000 and 800,000 cells/mL. After that, the prepared cells were moved into a growing cabinet. After discarding the spent culture media, Physiological Saline Solution (PBS) was used to wash the cells. There were two iterations of this washing procedure, each lasting ten minutes. A sufficient amount of trypsin enzyme was added to the cells, and they were incubated for 30 to 60 seconds at 37°C. The cells were monitored until they detached from a monolayer into individual cells. At this point, the action of the enzyme was halted by adding fresh culture medium containing fetal bovine serum. The cells were then collected into centrifuge tubes and centrifuged at 2000 rpm for 10 minutes at room temperature to pellet the cells and remove the trypsin and used culture medium. The supernatant was discarded, and the cells were resuspended in fresh culture medium containing 10% fetal bovine serum. Subsequently, a portion of the cell suspension was mixed with an equal volume of Trypan Blue stain to assess the total cell count and cell viability using a hemocytometer, following the equation below:

The cell concentration was calculated using the Eq. 1:

$C = N \times 10^4 \times F/ml$

Where:

C = Number of cells per milliliter

N = Number of cells counted in the hemocytometer

F = Dilution factor

10^4 = Hemocytometer's volume correction factor

The viability percentage of the cells in the sample was also determined using the hemocytometer, according to the following equation:

Cell Viability Percentage=Number of Dead Cells Number of Viable Cells × 100= Number of Viable Cells\ Number of Dead Cells ×100

The prepared cell suspension was then distributed into new culture vessels and incubated in a 5% carbon dioxide (CO_2) incubator at 37 °C for 24 hours.

Table 2. Weights, number of moles, and mole ratio of each of the nano ligand and metals.

Wt., mol (ligand)	Wt., mmol(metallics)					
DMTDP	$NiCL_2.6H_2O$	$CuCL_2.2H_2O$	$ZnCl_2$	$AgNO_3$	$CdCL_2.2H_2O$	$PdCl_2$
0.21 g,0.5mmol	0.12g,0.5mmol	0.08g,0.5mmol	0.06g,0.5mmol	0.08g,0.5mmol	0.11g,0.5mmol	0.08g,0.5mmol

Test the Dye of MTT to Examine the Vitality of Cells Principle of Testing

The cytotoxicity of the palladium complex was evaluated on MCF-7 breast cancer cells and compared with the normal HEK cell line to assess their toxicity on human cells and their potential use as anticancer agents.

The Method of Work

The cancer cell lines were prepared following the previously outlined steps. The cell suspension was then placed into a 96-well plate with a flat bottom, and the plate was incubated in a 5% CO_2 incubator at 37°C for 24 hours. After incubation, 100 µL of the cell suspension was added to each well. The prepared concentrations of the compounds under study (50 , 100 , 200 , 400 , 800 and 1600 µg/mL) were then added to the wells, with each concentration tested in triplicate· The plate was incubated again at 37°C for 24 hours· Following this, 10 µL of a 0·5 mg/mL solution of 3-(4,5-dimethylthiazol-2-yl)-2,5-diphenyltetrazolium bromide (MTT) was added to each well, and the plate was incubated for an additional four hours at 37°C. To dissolve the resulting formazan crystals, 100 µL of solubilization solution was added to each well. Finally, the absorbance of each sample was measured at a wavelength of 570 nm using a microplate reader (9602G-DNM). The absorbance is directly related to the number of viable cells in the medium. Cell viability was presented as a percentage relative to the viability of untreated cells.

RESULTS AND DISCUSSION

The nuclear magnetic resonance (NMR) spectroscopy was used to identify the placement of protons in the obtained nano ligand (DMTDP), ^{1}H-NMR (DMSO-d_6) Fig. 2a: The signal around (2.19 and 2.22 ppm) can be attributed to the methyl groups on the thiazole ring , while the methyl group linked to the azomethine group gave a single signal at (1.81 ppm). The protons of the aromatic rings in the prepared nano ligand showed multiple signals at the range (6.90 – 7.95 ppm) . The proton of the phenolic hydroxyl group() appears as a broad signal at (9.82 ppm). [14].^{13}C-NMR (DMSO-d_6) Fig. 2b: the carbon atoms of the methyl groups of the thiazole ring and the methyl group attached to the azomethine group showed signals at (10.32 , 14.64 and 26.32 ppm). The signals at (115.54 – 141.23 ppm), these signals are in the aromatic region, likely representing the carbons in the phenyl rings, with slight variations in shifts due to differences in the substitution pattern, the signals (122.61 , 151.54 and 171.27 ppm) may be attributed to the carbons in the thiazole ring, the signals of the carbon atoms of the azomethine groups were observed at (151.72 and 165.31) , (39.5-40.3 ppm ppm) these are the signals associated with the solvent DMSO-d_6 used in the NMR analysis [15, 16].

Mass Spectrum

The mass spectrum is used to confirm the chemical structure of the nano ligand (DMTDP). The mass spectrum of the nano ligand (DMTDP) showed multiple peaks shows the mass spectrum data in detail. The mass spectrometry shows Schiff's new base for a base peak at (m/z^{+}= 527), which mainly corresponds to the molecular weight of nano ligand (DMTDP) after losing one proton, while the other peaks are shown as follows:

The peak at (m/z = 269.1) This is the highest peak (Base Peak) in the spectrum, representing the most stable fragment of the molecule. It may

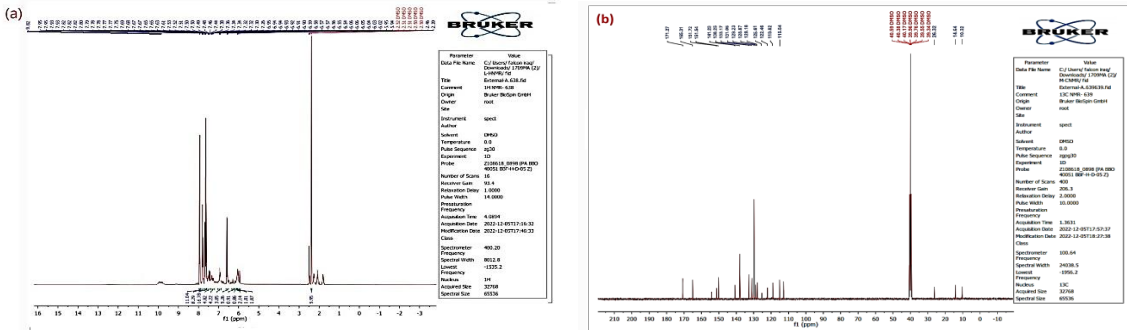

Fig. 2. (a) ^{1}H-NMR and ^{13}C-NMR (b) of (DMTDP)

result from the loss of heavy functional groups or partial fragmentation of the main molecule. (m/z = 120.1)This peak could be related to the fragmentation of the thiazole ring or part of the aromatic rings in the nano ligand. Signals in this range typically result from the breakdown of aromatic or heterocyclic structures.(m/z = 175.2) This peak might be associated with fragmentation involving part of the aromatic structures or a fragment that includes the imine group (-C=N) or the methyl group.(m/z = 224.2 and m/z = 254.2) These peaks could reflect major fragmentations in the molecule, possibly involving part of the aromatic system or functional groups attached, such as phenol or thiazole.(m/z = 392.3)The peak may result from further fragmentation of the core molecular structure or the loss of some heavy side groups.(m/z = 65.2 and m/z = 92.2)These peaks are typically associated with the fragmentation of benzene rings or other aromatic parts. These signals are likely from the complete breakdown of some aromatic rings in the nano ligand Fig. 3.

The main peak at m/z = 269.1 likely corresponds to a stable fragment of the decomposed nano ligand, potentially resulting from the loss of side groups such as phenol or thiazole. Other peaks indicate the fragmentation of various functional groups in the nano ligand, including aromatic rings, the imine group, and the thiazole ring. [17, 18].

FTIR spectra

Upon analyzing the FTIR spectra of the synthesized complexes of the (DMTDP) nano ligand and comparing them with the spectrum of the free ligand, several significant shifts, disappearances, and the appearance of new bands were observed. These changes provide evidence of coordination between the metal ion and the nano ligand, which can be explained as follows:

- Disappearance of the Phenolic Hydroxyl Group Band:

The absorption band corresponding to the hydroxyl group disappears, indicating the loss of its proton due to coordination with the metal ion. This is accompanied by the appearance of new bands in the range of 484-498 cm^{-1}, attributed to the (M-O) υ stretching vibrations in the spectra of the Ni(II) , Cu(II) and Ag(I) complexes.

- Shift of the Azomethine Group υ(C=N) Band:

The azomethine group, associated with the Schiff base, originally appeared at 1660 cm^{-1} in the spectrum of the free ligand. Upon coordination with the metal ions, this band either shifted to lower frequencies by approximately 10-18 cm^{-1}, reflecting the interaction between the metal ions and the azomethine nitrogen [19].

- Appearance of New Bands at 542-589 cm^{-1}:

These new bands are attributed to the (M-N) υ stretching vibrations, resulting from the coordination of the nano ligand with the metal ions through the nitrogen atoms of the azomethine group.

- Appearance of Broad New Bands at 3446,

Table 3. Infrared absorption bands of the prepared nano ligand (DMTDP) and its metal complexes

Compound	υ(O-H)	υ (C-H) aromatic	υ (C-H) aliphatic	υ(C=N) Imine	υ(C=N) thiazole	υ(C=C) aromatic	υ(M-N) υ(M-O)
Ligand (DMTDP)	3324 (O-H phenolic)	3062	2942 2859	1660	1600	1542 1488	- -
[Ni (DMTDP)$(H_2O)_2$Cl]	3446 (O-H aqua)	3062	2948 2889	1646	1604	1542 1488	582 498
[Cu (DMTDP)$(H_2O)_2$Cl]	3492 (O-H aqua)	3058	2923 2889	1650	1600	1554 1486	589 484
[Zn (DMTDP) Cl]	-	3062	2932 2862	1648	1598	1542 1488	572 -
[Pd (DMTDP) Cl]	-	3062	2972 2894	1646	1602	1542 1488	552 -
[Ag (DMTDP) (H_2O)]	3446 (O-H aqua)	3062	2954 2846	1648	1602	1542 1488	584 498
[Cd (DMTDP) Cl]	-	3062	2932 2862	1642	1604	1548 1494	542 -

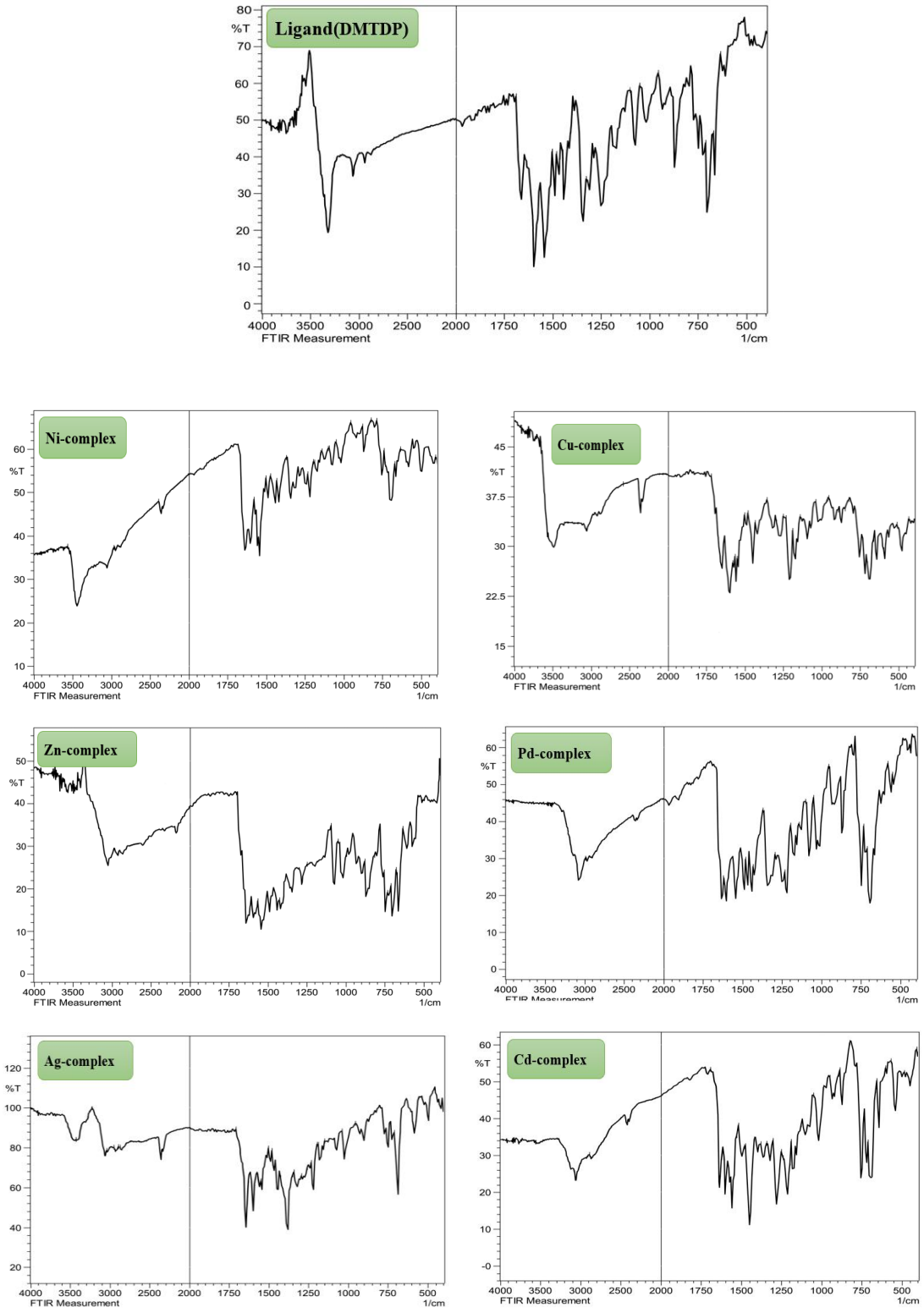

Fig. 4. FT-IR spectra of complexes

3492, and 3446 cm^{-1}:

These broad bands correspond to the hydroxyl groups of the coordinated water molecules in the spectra of the nickel(II), copper(II), and silver (I) complexes, respectively[20] , Table 3 and Fig. 4.

Stability Studies of Metal Complexes Solutions
Studying effect of solvent

To determine the most suitable solvent for use during the synthesis of the nano ligand and its metal complexes, as well as for conducting subsequent laboratory measurements, the effect of various solvents was studied. The solvents examined included ethanol (EtOH), methanol (MeOH), dimethyl sulfoxide (DMSO), dimethylformamide (DMF), acetone, and formic acid. The UV-Vis spectrum of the nano ligand, measured at optimal concentration and room temperature, showed that the solvent choice significantly affected the maximum wavelength (λmax) values due to the polarity of the solvents used. The Table 4 presents the absorption values obtained, which reveal clear differences in the λ_{max} of the nano ligand across the different solvents.

When analyzing these differences, some interpretations can be made. The position of the azo group may be influenced by tautomeric phenomena and the various groups attached to the nano ligand. Additionally, the intramolecular hydrogen bonding, commonly observed in organic compounds, can be identified by the blue shift in the λmax when the solvent is changed. The λmax of the nano ligand is also affected by the presence of aromatic rings, particularly the π–π* and n–π* electronic transitions, which vary with solvent polarity. Moreover, the dielectric constant and refractive index of the solvents play a significant role in altering the absorption peak position of the nano ligand. The spectra of the nano ligand in the aforementioned solvents are shown in Fig. 5. Ethanol was found to be the most suitable solvent for the preparation of the metal complexes during laboratory measurements.

This table illustrates the maximum absorption wavelengths (λ_{max}) and corresponding absorbance values of the nano ligand in various solvents.

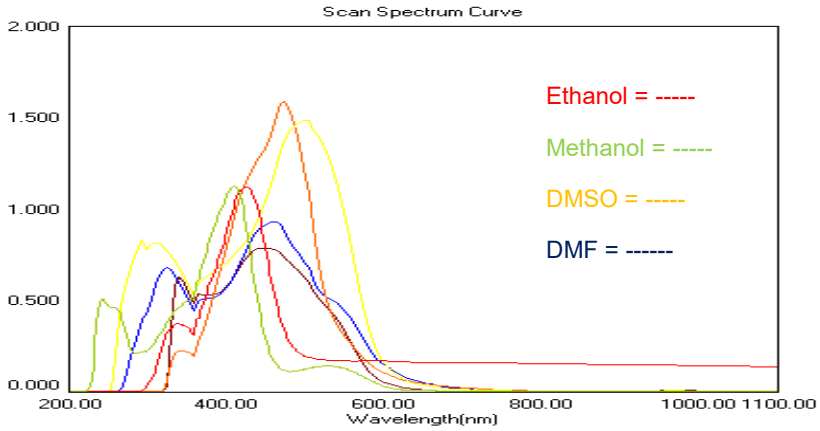

Fig. 5. UV-visible spectra of the nano ligand (DMTDP) using different solvents

Table 4. Maximum Absorption Values of the Nano Ligand (DMTDP) Using Different Solvents

Ligand	Solvent	λ_{max} (nm)	Absorbance
DMTDP	Ethanol (EtOH)	426	1.593
	Methanol (MeOH)	412	1.129
	Dimethylformamide (DMF)	465	0.932
	Dimethyl sulfoxide (DMSO)	475	1.121
	Acetone	445	0.788
	Formic acid	500	1.486

Each solvent shows a distinct λ_{max}, indicating the influence of solvent polarity and other properties on the nano ligand electronic transitions[21, 22].

Determination of M: L Ratio for Synthesized Complexes

One of the most effective methods for researchers to determine the possible structural formula of complexes is through the use of UV-Visible spectroscopy on solutions of chelate complexes. Several techniques are employed to determine the metal-to-ligand ratio, with some of the most common spectroscopic methods being:

1. Mole Ratio Method: This method, introduced by Yoe and Jones, was utilized in our current study to determine the metal-to-ligand ratio in the complexes.

2. Job's Method or Continuous Variation Method: This technique was developed by Vosbury and Coobury.

Among these, the mole ratio method is considered superior and is the most widely used

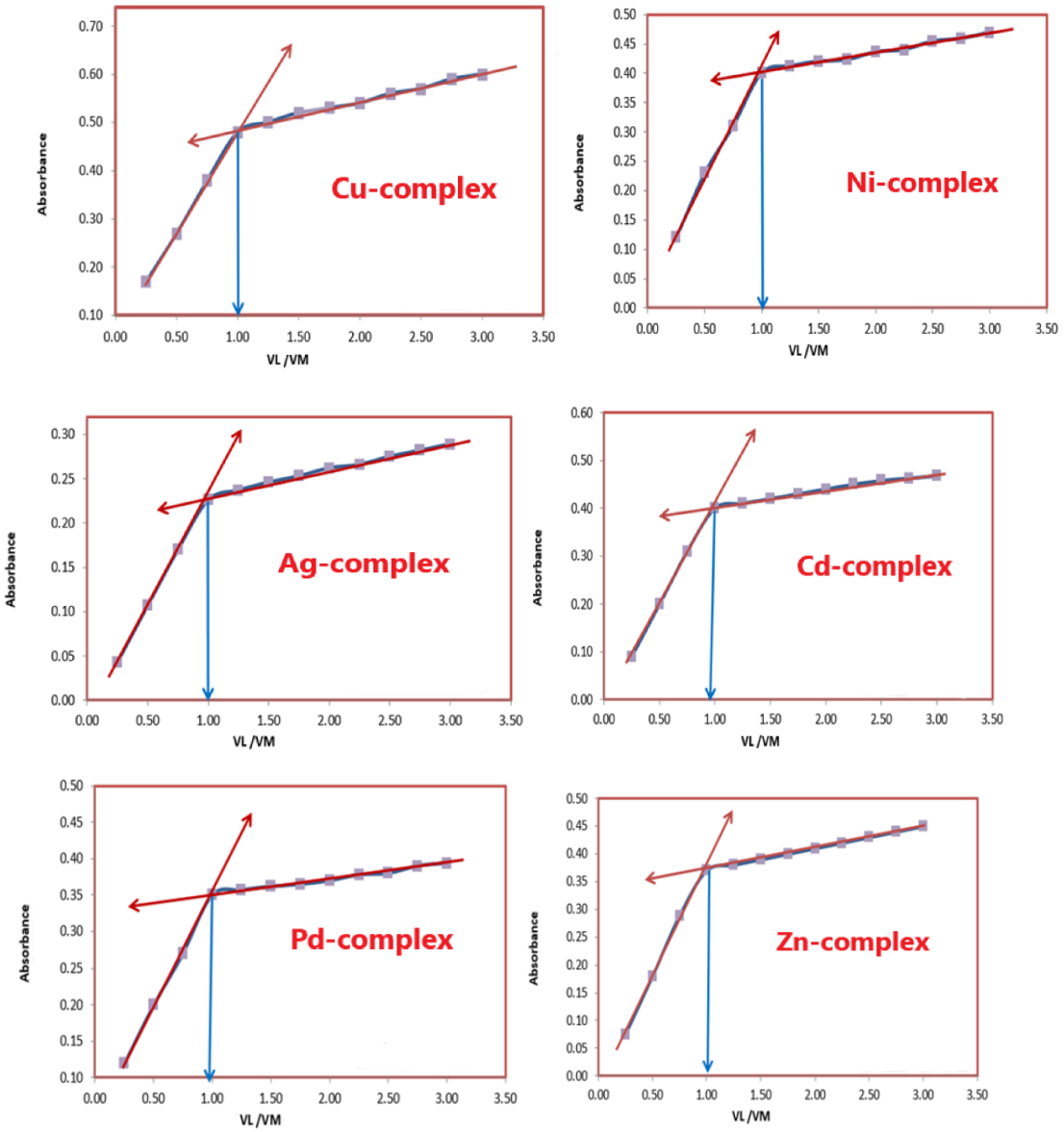

Fig. 6. Molar ratio curves of nano ligand (DMTDP) complexes.

because it provides the most reliable results with ligands and is simple to perform. The procedure used in our study to determine the metal-to-ligand ratio is summarized as follows:

A series of solutions were prepared with varying molar concentrations of the metal ions, keeping the metal quantity constant while incrementally increasing the amount of the ligand each time. The absorbance was then measured against the mole ratio at the maximum wavelength ($\boldsymbol{\lambda}_{max}$) of the complex. The relationship between absorbance and the mole ratio of ligand to metal was plotted, resulting in two straight lines. The intersection of these lines represents the metal-to-ligand ratio in the complex. Fig. 6 illustrate the graphical curves obtained for the solutions of Ni(II), Cu(II), Zn(II), Ag(I), Cd(II), and Pd(II) ions, respectively, with the ligand (DMTDP).

The intersection points of the straight lines represent the metal-to-ligand ratio in the complex. From these curves, it can be observed that the molar ratio for all the metal complexes is 1:1 [M:L] [23-25].

Molar Conductivity

Molar conductivity is one of the most important techniques used to determine the ionic nature of metal complexes in coordination chemistry. It is currently the only method available to ascertain the ionic formula of complexes.

Molar conductivity is directly proportional to the number of ions in solution and increases with the number of free ions of the complex in the solution (Table 5). When the conductivity value of a solution is close to zero, the solution is considered non-ionic. Conversely, if the conductivity value is high, the complex in solution exhibits ionic characteristics.

In many cases, organic solvents such as dimethyl sulfoxide (DMSO), dimethylformamide (DMF), ethanol, methyl cyanide, and nitromethane are used to measure the molar conductivity of coordination compounds. These solvents are chosen because they are inert towards the complexes and have a high dielectric constant and low viscosity. On the other hand, water is rarely used as a solvent in this measurement due to the

Table 5. Molar Conductivity Values for Compounds in Various Solvents Across Specific Ranges

Solvent	Non-Electrolyte	Electrolyte Type			
		1:1	1:2	1:3	1:4
Water	0.0	120	240	360	480
DMSO	0 – 20	30 - 40	70 – 80	-----	------
DMF	0 – 30	65 - 90	130 – 170	200 – 240	300
Ethanol	0 – 20	35 - 45	70 – 90	120	160
Nitro Methane	0 – 20	75 - 95	150-180	220-260	290-330
Methyl Cyanide	0 – 30	120-160	220-300	340-420	500

Table 6. Molar Conductivity ($Ohm^{-1}\cdot cm^2\cdot mol^{-1}$) for Nano Ligand (DMTDP) and Its Complexes at 10^{-3} Molar Concentration and Room Temperature

No.	Complex	Λ ($Ohm^{-1}\cdot cm^2\cdot mol^{-1}$)	Ionic Ratio
1	[Ni (DMTDP)$(H_2O)_2$Cl]	12.4	Non-Ionic
2	[Cu (DMTDP)$(H_2O)_2$Cl]	14.3	Non-Ionic
3	[Zn (DMTDP) Cl]	15.1	Non-Ionic
4	[Pd (DMTDP) Cl]	11.5	Non-Ionic
5	[Ag (DMTDP) (H_2O)]	7.2	Non-Ionic
6	[Cd (DMTDP) Cl]	10.3	Non-Ionic

potential dissociation of the complexes or their poor solubility in water.

The molar conductivity of the synthesized chemical compounds was measured to determine the ionic formula of these coordination complexes and to identify whether the ions are present inside

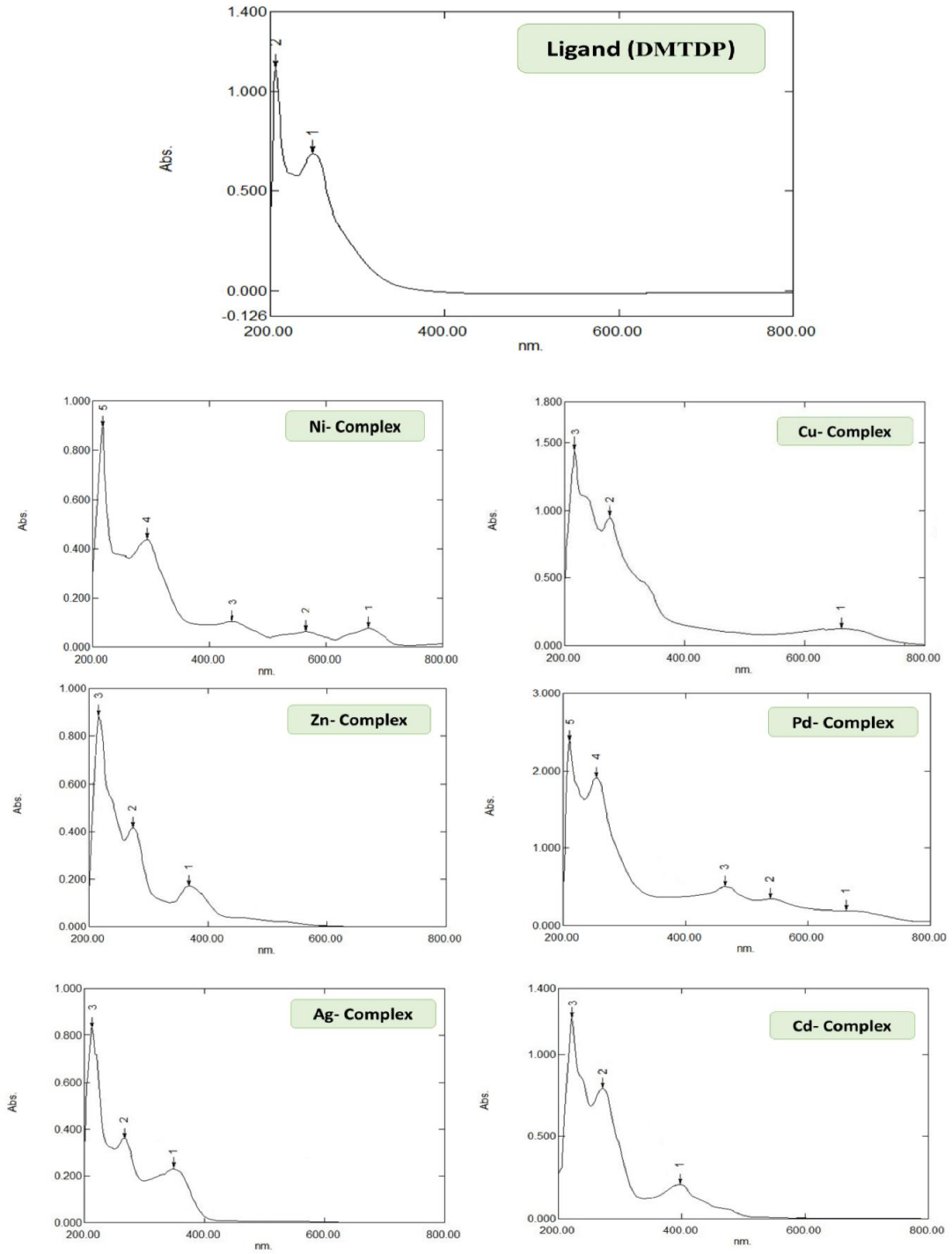

Fig. 7. The electronic spectrum of the complexes

or outside the coordination sphere (Table 6). Absolute ethanol was used as the solvent for the nano ligand complexes (DMTDP) at a concentration of 10^{-3} M and at room temperature. The molar conductivity measurements in the solvent were consistent with the proposed formulas of the complexes[26, 27].

These values confirm that the complexes primarily exhibit non-ionic characteristics for all complexes.

Electronic Spectrum

The solutions of transition metal complexes are characterized by their vibrant colors due to the presence of functional groups known as chromophores. These chromophores are responsible for absorption in the visible region of the spectrum, accompanied by additional absorptions in the regions near the infrared and ultraviolet. This behavior is due to the partially filled (d) orbitals of the atoms or ions of these transition metals. Table 7 and Fig. 7 displays the electronic spectrum of the nickel (II) complex, which exhibited several peaks at 214 nm (46729 cm^{-1}) and 289 nm (34602 cm^{-1}). These peaks are attributed to intra-ligand transitions, which were slightly red-shifted compared to the free ligand spectrum due to coordination between the ligand and the metal ion. Absorption peaks at 436 nm (22936 cm^{-1}), 564nm (17730 cm^{-1}) and 674 nm (14837 cm^{-1}) correspond to the electronic transitions ^3A_2g (F) $\rightarrow ^3T_2g$(F), ^3A_2g (F) $\rightarrow ^3T_1g$,^3A_2g (F) $\rightarrow ^3T_1g$ (P), respectively, indicating that the nickel (II) complex has an octahedral geometry. The electronic spectrum of the copper (II) complex, which revealed three absorption peaks at 215 nm (46512 cm^{-1}) and 273 nm (36630 cm^{-1}) all attributed to intra-ligand transitions. A broad absorption band at 664 nm (15060 cm^{-1}) is assigned to $^2B_1g \rightarrow ^2Eg$ transition, which appears as a broad band due to Jahn-Teller distortions, indicating a distorted octahedral geometry for the copper (II) complex. The electronic spectrum of the palladium (II) complex, which showed

Table 7. Absorption values of the ultraviolet-visible spectrum, magnetic moment, and expected geometry of the nano ligand (DMTDP) and its complexes

Compounds	λ (nm)	υ⁻ (cm^{-1})	Transitions	μeff (B.M)	Geometry
Ligand (DMTDP)	202	49505	π-π*	-	-
	248	40323	n-π*		
[Ni (DMTDP)(H_2O)$_2$Cl]	214	46729	Intra Ligand	2.81 (Para.)	Octahedral sp^3d^2 Regular
	289	34602	Intra Ligand		
	436	22936	^3A_2g (F) $\rightarrow ^3T_1g$ (P)		
	564	17730	^3A_2g (F) $\rightarrow ^3T_1g$(F)		
	674	14837	^3A_2g (F) $\rightarrow ^3T_2g$(F)		
[Cu (DMTDP)(H_2O)$_2$Cl]	215	46512	Intra Ligand	1.73 (Para.)	Octahedral sp^3d^2 distorted
	273	36630	Intra Ligand		
	664	15060	$^2B_1g \rightarrow ^2Eg$		
[Zn (DMTDP) Cl]	216	46296	Intra Ligand	(Dia.)	Tetrahedral sp^3
	272	36765	Intra Ligand		
	368	27174	Charge transfer(MLCT)		
[Pd (DMTDP) Cl]	212	47170	Intra Ligand	(Dia.)	Square planar dsp^2
	254	39370	Intra Ligand		
	467	21413	$^1A_1g \rightarrow ^1Eg$		
	536	18657	$^1A_1g \rightarrow ^1B_1g$		
	662	15106	$^1A_1g \rightarrow ^1A_2g$		
[Ag (DMTDP) (H_2O)]	213	46948	Intra Ligand	(Dia.)	Tetrahedral sp^3
	268	37313	Intra Ligand		
	397	25189	Charge transfer(MLCT)		
[Cd (DMTDP) Cl]	221	45249	Intra Ligand	(Dia.)	Tetrahedral sp^3
	274	36496	Intra Ligand		
	398	25126	Charge transfer(MLCT)		

absorption peaks at 212 nm (47170cm^{-1}) and 254 nm (39370cm^{-1}) all corresponding to intra-ligand transitions. Additional peaks at 467 nm (21413 cm^{-1}), 536 nm (18657 cm^{-1}), and 662 nm (15106 cm^{-1}) are attributed to the electronic transitions $^1A_1g \rightarrow {}^1Eg$, $^1A_1g \rightarrow {}^1B_1g$ and $^1A_1g \rightarrow {}^1A_2g$, respectively, indicating that the palladium (II) complex has a square-planar geometry. The electronic spectra of the zinc (II), silver (I), and cadmium (II) complexes did not display any (d-d) transitions due to the fully occupied (d) orbitals, which prevents the use of their electronic spectra to determine the geometry. However, these complexes exhibited several peaks in the range of 213-274 nm (46948 – 36496 cm^{-1}), attributed to intra-ligand transitions. Peaks at 368, 397, and 398 nm (27174 , 25189 and 25126 cm^{-1}), respectively, correspond to metal-to-ligand charge transfer (M → L) transitions in the zinc (II), silver (I), and cadmium (II) complexes. Previous studies have confirmed that these complexes possess tetrahedral geometries[28-30].

X-ray diffraction (XRD)

The crystal structures of the complexes in their solid state were analyzed using X-ray diffraction within the angular range (2θ) of 10° to 80°. Through this diffraction analysis, the crystal structure and crystallite size were determined, along with the purity of the synthesized compounds. X-ray diffraction peaks are occasionally influenced by various factors, leading to broadening of the peaks in some cases. This broadening is attributed to micro-strains, such as lattice deformation, crystal faulting, crystal size, and the distribution of domain size.

Observation of the X-ray diffraction patterns revealed that sharp peaks indicate the formation of a crystalline or semi-crystalline structure, confirming the crystalline nature of the compound. In contrast, broad and non-distinct peaks suggest that the compound possesses an amorphous structure. The crystallite size or the interplanar spacing (d) was calculated using Bragg's Law.

The variable d represents the interplanar spacing between crystal planes, while n is the order of reflection (with values such as 1, 2, 3, ...). The wavelength (λ) of the X-ray used in the diffraction experiment is 1.540598 Å, and θ refers to the angle of diffraction.

Bragg's Law is applied in this context to

Table 8. Diffraction angles, full width at half maximum (FWHM) of the peaks, crystallite size (D), relative intensity, and lattice strain for the DMTDP and its metal complexes.

Compound	No.	Peak Position °2θ	Peak Width (FWHM)	D Crystallite size(nm)	Rel. Int [%]	Lattice Strain
DMTDP	1	17.54	0.5610	14.328	100	0.0154
	2	24.65	0.6398	12.710	34.75	0.0126
	3	23.27	0.4823	16.817	25.79	0.0101
Ni- complex	1	18.43	0.1674	48.077	100	0.0043
	2	37.53	0.1868	44.916	40.25	0.0025
	3	47.81	0.2462	35.295	28.21	0.0023
Cu- complex	1	16.38	0.1674	47.946	100	0.0048
	2	33.82	0.2462	33.726	23.71	0.0034
	3	57.46	0.3249	27.884	11.33	0.0025
Zn- complex	1	17.84	0.3642	22.080	100	0.0099
	2	20.93	0.4823	16.750	57.220	0.0112
	3	11.67	0.2462	32.436	19.84	0.0102
Pd- complex	1	16.24	0.1674	47.938	100.00	0.0048
	2	28.98	0.2855	28.740	30.42	0.0047
	3	44.94	0.9546	9.006	13.26	0.0100
Ag- complex	1	38.15	0.2462	34.142	100	0.0030
	2	44.47	0.1674	51.269	35.27	0.0017
	3	64.62	0.2462	38.179	23.45	0.0016
Cd- complex	1	15.16	0.1674	47.875	100	0.0052
	2	37.18	0.1281	65.430	71.28	0.0015
	3	46.54	0.2462	35.125	50.53	0.0024

determine the interplanar spacing[31], where the Eq. 2 is given as:

$$d = \frac{n\lambda}{2\sin\theta} \quad (2)$$

This formula is crucial for analyzing the crystal structure and determining the distance between crystal planes as shown in the Fig. 8 and Table 8.

X-ray diffraction (XRD) measurements indicated that the synthesized complexes possess a crystalline structure, as all observed peaks were sharp. When the intensity and positions of the peaks were compared with standard reference cards from the International Centre for Diffraction Data (ICDD), it was confirmed that these positions correspond to the primary compounds from which the studied complexes were derived. No unexpected peaks or signals related to extraneous materials were observed. Based on the XRD data, it was evident that all the synthesized materials exhibit a nanoscale nature, as the crystallite sizes of these complexes were found to be less than 100 nanometers [32, 33].

According to the X-ray diffraction (XRD) results calculated using the Scherrer equation, the crystallite sizes for the DMTDP and its metal complexes . (DMTDP)The crystallite sizes range between 12.7 nm at a 2θ angle of 24.65° and 16.8 nm at a 2θ angle of 23.27°. This indicates that the nano ligand exhibits a nanostructure with relatively small crystallite sizes, suggesting a structure with wide atomic dispersion.(Nickel Complex) The complex shows larger crystallite sizes compared to the nano ligand, ranging from 35.3 nm at a 2θ angle of 47.81° to 48.1 nm at a 2θ angle of 18.43°. This suggests the formation of more regular and larger crystallites after coordination with nickel. (Copper Complex) The crystallite sizes for the complex range around 27.9 nm at the highest angle (57.46°), while reaching up to 47.9 nm at the lowest angle (16.38°). This indicates variability in crystallite size depending on the diffraction angle, with larger crystallites at lower angles.(Zinc Complex) The crystallite sizes range between 16.8 nm and 32.4 nm, indicating that the crystallite sizes tend to be smaller than the nickel complex but with similar nanoscale characteristics to the other complexes.(Palladium Complex) The crystallite size was measured at around 9.0 nm at a 2θ angle of 44.94°, which is the smallest crystallite size among all the complexes. This suggests that the palladium complex contains much smaller and denser crystalline structures.(Silver Complex) The complex exhibited crystallite sizes ranging from 34.1 nm to 51.3 nm, showing variability in crystallite size with relatively larger crystallites at smaller diffraction angles.(Cadmium Complex) The cadmium complex exhibited the largest crystallite size at a 2θ angle of 37.18°, measuring around 65.4 nm, making it the complex with the largest crystallite size in the study. This indicates the presence of large and relatively well-ordered crystallites compared to the other complexes. These results indicate that the formation of metal complexes from the nano ligand caused significant changes in the crystallite size for each complex, reflecting the influence of different metals on the compound's structure and crystallinity.

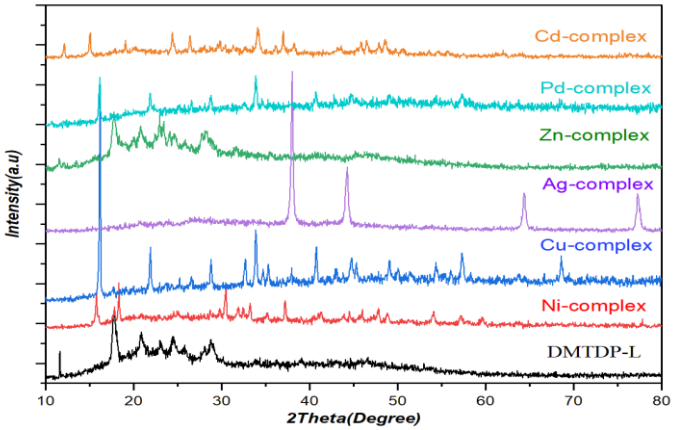

Fig. 8. XRD of the DMTDP and complexes

Scanning Electron Microscopy (SEM)

Using scanning electron microscopy (SEM), information on the surface morphology, particle size, shape, and crystalline structure of the complexes can be obtained. SEM is one of the most important techniques for gathering such data, as the properties and activity of both the nano ligands and complexes depend on surface morphology and characteristics. In this study, SEM analysis was performed with a cross-sectional

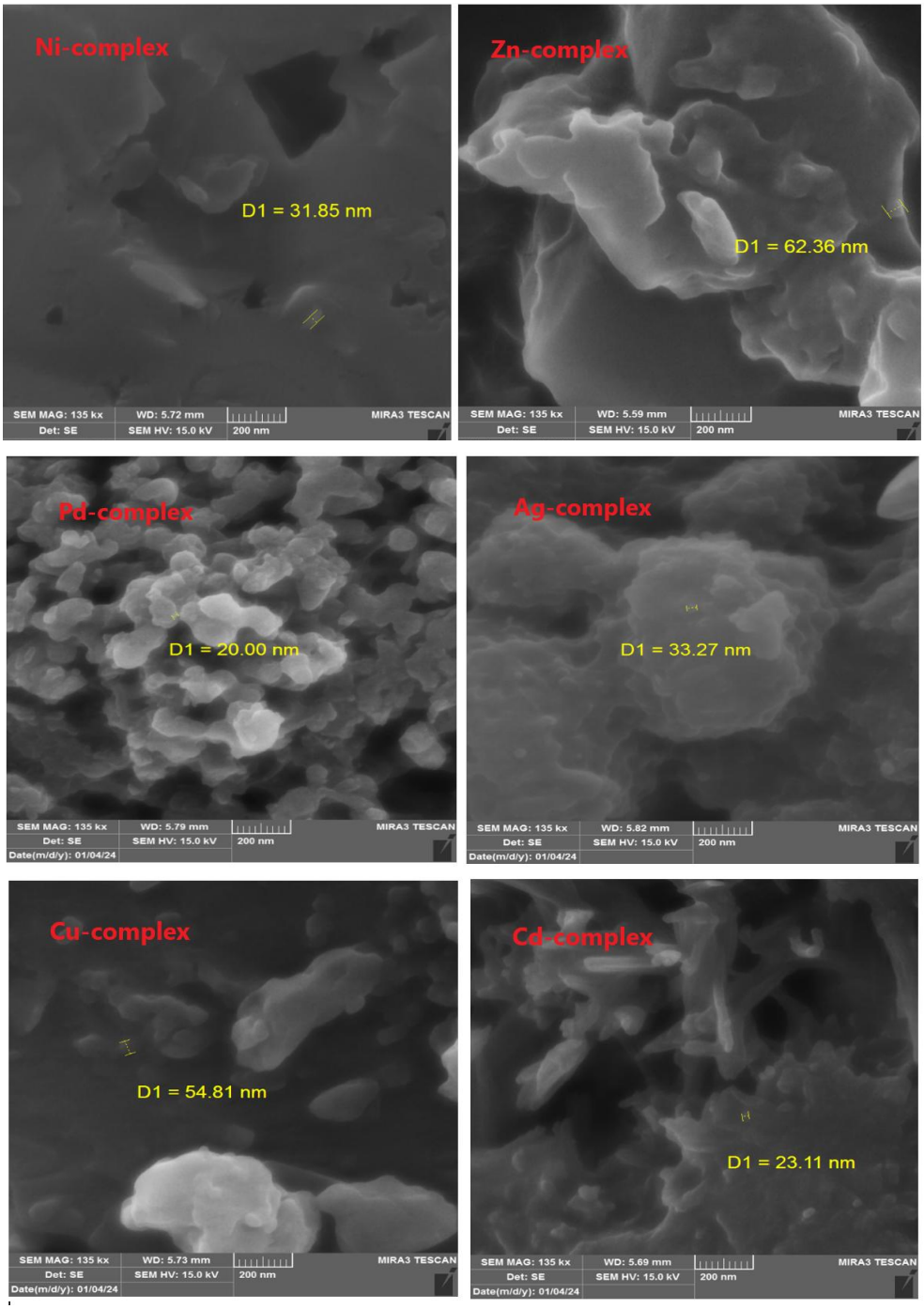

Fig. 9. Scanning electron microscope images of each of the metal complexes

distance of 200 nm and a magnification of 135 KX.

Fig. 9: Scanning electron microscope (SEM) images of each of the synthesized metal complexes, showing the granular morphology of the particles within the nanoscale range. The images illustrate the surface characteristics, particle size, and shape for each complex. Nickel (II) Complex: Irregular, semi-spherical particles with an average size of 31.85 nm.Copper (II) Complex: Small, surface-heterogeneous particles with an average size of 54.81 nm.Zinc (II) Complex: Non-uniform particles with an average size of 62.36 nm.Palladium (II) Complex: Very small, spherical particles with an average size of 20 nm, unevenly distributed. Silver (I) Complex: Small, spherical particles in uniform clusters with an average size of 33.27 nm.Cadmium (II) Complex: Small, semi-spherical aggregated particles with an average size of 23.11 nm. Each image demonstrates the granular and nanoscale nature of the complexes, supporting their potential applications in various fields[34].

The results of our study using scanning electron microscopy revealed that the metal complexes synthesized from the nano ligand exhibit a granular morphology and fall within the nanoscale range, with an average particle size of less than 100 nanometers. Due to this nanoscale size, the active surface area is significantly increased, which

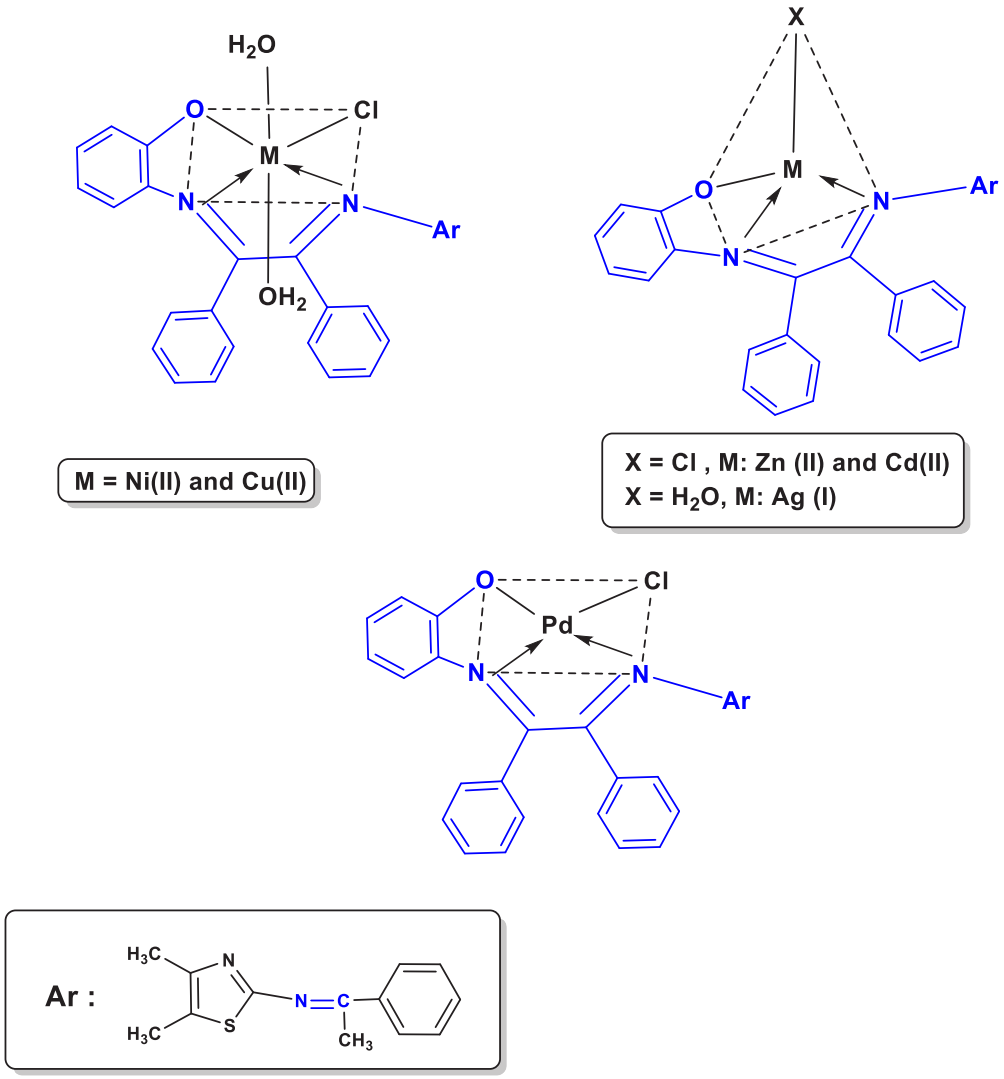

Fig. 10. The proposed stereoscopic shape of the nano ligand complexes (DMTDP)

contributes to the quantum effect of creating new energy levels. This enhances the free movement of electrons, providing substantial benefits due to the properties that allow these complexes to be applied in industrial fields, such as thermal or electrical conductivity, as well as in medical and pharmaceutical fields for the treatment of certain types of cancer[35].

The Proposed Structural Formula of the Complexes

The measurements conducted on the nano ligand have confirmed the proposed geometries of the complexes. It was established that the geometry of the nickel (II) and copper (II) complexes is octahedral, while the zinc (II), cadmium (II), and silver (I) complexes exhibit a tetrahedral structure (Fig. 10). The palladium (II) complex adopts a square planar geometry. The structures proposed for these complexes are illustrated below. The ligand coordinates with the metal ions through the nitrogen atoms of the azomethine group, the nitrogen atom of the azomethine group in the thiazole ring, and the oxygen atom of the hydroxyl group after the loss of its proton. Thus, the ligand acts as a tetradentate ligand[36].

Biological Activity

The biological activity of the synthesized nano ligand complexes was evaluated by preparing solutions in dimethyl sulfoxide (DMSO) and testing them against two types of pathogenic bacteria: one Gram-positive and one Gram-negative. Gram staining is used to differentiate these bacteria; Gram-positive bacteria retain the stain and absorb it into their cell walls, while Gram-negative bacteria expel the stain due to their thinner cell walls and higher lipid content. Because of this difference, the two bacterial strains used in this study were the Gram-negative Escherichia coli and the Gram-positive Staphylococcus aureus. [37] A concentration of 500 ppm of the compound solutions in DMSO was used, and the following results were obtained for the complexes in Table 9.

The Table 9 displays the effects of the nano ligand (DMTDP) and its various complexes against two types of bacteria: Staphylococcus aureus (S. aureus) and Escherichia coli (E. coli) at a concentration of 500 ppm. The effectiveness is measured by the inhibition zone, indicating the ability of the nano ligand and complexes to inhibit bacterial growth. Table 9 values represent the

Table 9. Inhibition Zones of Complexes *Against S. aureusand E. coli* (in mm)

No.	Complex	S. aureus (500 ppm)	E. coli (500 ppm)
1	(DMTDP)	11	7
2	[Ni(DMTDP)(H_2O)Cl]	10	5
3	[Cu(DMTDP)(H_2O)Cl]	5	6
4	[Zn(DMTDP)]Cl	11	5
5	[Pd(DMTDP)]Cl·H_2O	12	10
6	[Ag(DMTDP)]	7	10
7	[Cd(DMTDP)]Cl	11	4

Table 10. Effect of Palladium (II) Complex on Breast Cancer Cell Line (MCF-7) Compared to Normal Cell Line (Hek-293) at Various Concentrations Using the MTT Assay Over 24 Hours

Conc. µg/ml	Cancer cell MCF-7			Normal cell Hek-293		
	Cell Viability		Cell Inhibition %	Cell Viability		Cell Inhibition %
	Mean	SD		Mean	SD	
0	100	0	0	100	0	0
50	80.8	1.2727	19.2	73.8	0.8485	26.2
100	56.15	0.7778	43.85	53.8	2.1213	46.2
200	31.85	2.6162	68.15	40.2	7.0286	59.8
400	25.45	1.767	74.55	31.5	4.7376	68.5
800	21.35	0.9192	78.65	29	0.7071	71
1600	6.45	0.3535	93.55	21.25	0.9192	78.75
IC50	23.4			67.5		

diameter (in millimeters) of the inhibition zone around the sample. The Palladium (Pd(II)) complex shows the best effectiveness against both bacterial strains, making it the most promising antibacterial candidate.The Silver (Ag(I)) complex exhibited relatively high activity against E. coli compared to the other complexes.The Cadmium (Cd(II)) and Nickel (Ni(II)) complexes demonstrated good activity against S. aureus but weak against E. coli. The Copper (Cu(II)) complex was the least effective against S. aureus, indicating lower antibacterial activity compared to the other complexes[38].

Cell viability and Cytotoxicity Assay (MTT)

The breast cancer cell line MCF7 and the normal cell line HEK were exposed for comparison purposes, to study the effects of some synthesized compounds on both cancerous and normal cells. Concentrations ranging from 50 to 1600 µg/mL of the palladium(II) complex were used for 48 hours at a temperature of 37°C. The cytotoxic effects were evaluated by calculating the percentage inhibition rate of cell growth, compared to the control group, which was considered to have 100% growth. The results showed that the type and concentration of the synthesized compounds played a significant role in determining the inhibition rate of the cells. The inhibition was highly dependent on concentration and other factors, a phenomenon known as dose dependence (Table 10). This observation aligns with findings from several other researchers[39-41].

Cancer Cell MCF-7:At a concentration of 50 µg/mL, the cancer cell viability was 80.8%, with an inhibition rate of 19.2%.As the concentration increased, the inhibition rate rose significantly, reaching 93.55% at 1600 µg/mL, with only 6.45% viable cells remaining.The IC50 for the MCF-7 cancer cells was calculated to be 23.4 µg/mL, indicating that this concentration is required to inhibit 50% of the cancer cells.

Normal Cell Hek-293:The normal cells showed a viability of 73.8% at 50 µg/mL, with an inhibition rate of 26.2%.The inhibition rate gradually increased with higher concentrations, reaching 78.75% at 1600 µg/mL.The IC50 for normal cells (Hek-293) was 67.5 µg/mL, which is higher than that of the cancer cells, indicating that the normal cells are less sensitive to the palladium complex compared to the MCF-7 cancer cells.

The palladium (II) complex demonstrates significant cytotoxicity against the MCF-7 breast cancer cell line, with an IC50 of 23.4 µg/mL. The normal cell line (Hek-293) is less affected, with an IC50 of 67.5 µg/mL, indicating that the complex may selectively target cancer cells. These results suggest that the palladium (II) complex has potential as an anticancer agent, but further adjustments may be required to minimize its effect on healthy cells.

CONCLUSION

The synthesized Schiff base metal complexes exhibited diverse biological activities, with the palladium complex demonstrating the most promising antibacterial and anticancer properties. The coordination of the DMTDP ligand with metal ions significantly impacted both the structural properties and the biological efficacy of the complexes. The palladium complex showed strong cytotoxicity against the MCF-7 breast cancer cell line with minimal impact on normal HEK cells, indicating its potential as a selective anticancer agent. However, further optimization is needed to improve its selectivity and reduce toxicity towards healthy cells. These findings contribute to the growing body of research on Schiff base complexes as potential therapeutic agents for cancer and bacterial infections.

CONFLICT OF INTEREST

The authors declare that there is no conflict of interests regarding the publication of this manuscript.

REFERENCES

1. Hameed A, al-Rashida M, Uroos M, Abid Ali S, Khan KM. Schiff bases in medicinal chemistry: a patent review (2010-2015). Expert Opin Ther Pat. 2016;27(1):63-79.
2. Boulechfar C, Ferkous H, Delimi A, Djedouani A, Kahlouche A, Boublia A, et al. Schiff bases and their metal Complexes: A review on the history, synthesis, and applications. Inorg Chem Commun. 2023;150:110451.
3. Uddin MN, Ahmed SS, Alam SMR. REVIEW: Biomedical applications of Schiff base metal complexes. J Coord Chem. 2020;73(23):3109-3149.
4. Khan S, Chen X, Almahri A, Allehyani ES, Alhumaydhi FA, Ibrahim MM, et al. Recent developments in fluorescent and colorimetric chemosensors based on schiff bases for metallic cations detection: A review. Journal of Environmental Chemical Engineering. 2021;9(6):106381.
5. Malav R, Ray S. Recent developments on the synthesis of copper and cobalt-Schiff base complexes and their assessment as anti-tuberculosis drugs. Chemical Papers. 2024;78(8):4623-4646.
6. Sarigul M, Erkan Kariper S, Deveci P, Atabey H, Karakas D, Kurtoglu M. Multi-properties of a new azo-Schiff base and its binuclear copper(II) chelate: Preparation,

spectral characterization, electrochemical, potentiometric and modeling studies. Journal of Molecular Structure. 2017;1149:520-529.
7. Youssef NS, El-Zahany EA, El-Seidy AMA. Synthesis and Characterization of New Schiff Base Metal Complexes and Their Use as Catalysts for Olefin Cyclopropanation. Phosphorus, Sulfur, and Silicon and the Related Elements. 2010;185(4):785-798.
8. Alizadeh SR, Hashemi SM. Development and therapeutic potential of 2-aminothiazole derivatives in anticancer drug discovery. Medicinal chemistry research : an international journal for rapid communications on design and mechanisms of action of biologically active agents. 2021;30(4):771-806.
9. Wan Y, Long J, Gao H, Tang Z. 2-Aminothiazole: A privileged scaffold for the discovery of anti-cancer agents. Eur J Med Chem. 2021;210:112953.
10. Shakir M, Hanif S, Sherwani MA, Mohammad O, Azam M, Al-Resayes SI. Pharmacophore hybrid approach of new modulated bis-diimine CuII/ZnII complexes based on 5-chloro Isatin Schiff base derivatives: Synthesis, spectral studies and comparative biological assessment. J Photochem Photobiol B: Biol. 2016;157:39-56.
11. Fahmy HM, Mosleh AM, El-Sayed AA, El-Sherif AA. Novel palladium(II) and Zinc(II) Schiff base complexes: Synthesis, biophysical studies, and anticancer activity investigation. Journal of Trace Elements in Medicine and Biology. 2023;79:127236.
12. PrabhuKumar KM, Satheesh CE, RaghavendraKumar P, Kumar MN, Lingaraju K, Suchetan PA, Rajanaika H. Synthesis, characterization, antibacterial, antifungal and antithrombotic activity studies of new chiral selenated Schiff bases and their Pd complexes. Journal of Molecular Structure. 2022;1264:133172.
13. Basaran E, Gamze Sogukomerogullari H, Cakmak R, Akkoc S, Taskin-Tok T, Köse A. Novel chiral Schiff base Palladium(II), Nickel(II), Copper(II) and Iron(II) complexes: Synthesis, characterization, anticancer activity and molecular docking studies. Bioorg Chem. 2022;129:106176.
14. Bharti SK, Nath G, Tilak R, Singh SK. Synthesis, anti-bacterial and anti-fungal activities of some novel Schiff bases containing 2,4-disubstituted thiazole ring. Eur J Med Chem. 2010;45(2):651-660.
15. Issa YM, Hassib HB, Abdelaal HE. 1H NMR, 13C NMR and mass spectral studies of some Schiff bases derived from 3-amino-1,2,4-triazole. Spectrochimica Acta Part A: Molecular and Biomolecular Spectroscopy. 2009;74(4):902-910.
16. More PG, Karale NN, Lawand AS, Narang N, Patil RH. Synthesis and anti-biofilm activity of thiazole Schiff bases. Med Chem Res. 2013;23(2):790-799.
17. Yernale NG, Udayagiri MD, Mruthyunjayaswam BHM. Synthesis, characterization, mass spectral fragmentation, thermal study and biological evaluation of new Schiff base ligand and its metal(II) complexes derived from 4-(diethylamino)salicylaldehyde and thiazole moiety. European Journal of Chemistry. 2016;7(1):56-65.
18. Khedr AM, El-Ghamry HA, Wahdan KM, Mandour HSA. Synthesis, characterization, antimicrobial, molecular docking simulation, and antitumor assays of nanometric complexes based on new thiazole Schiff base derivative. Appl Organomet Chem. 2024;38(3).
19. Lemilemu F, Bitew M, Demissie TB, Eswaramoorthy R, Endale M. Synthesis, antibacterial and antioxidant activities of Thiazole-based Schiff base derivatives: a combined experimental and computational study. BMC chemistry. 2021;15(1):67-67.
20. Sail BS, Naik VH, Prasanna BM, Ahmad N, Khan MR, Jagadeesh MR, et al. Synthesis, characterization and pharmacological studies of cobalt(II), nickel (II) and copper (II) complexes of thiazole schiff bases. Journal of Molecular Structure. 2023;1288:135748.
21. Upadhyay A, Kar PK, Dash S. A spectrophotometric study of impact of solvent, substituent and cross-conjugation in some 4-aminoantipyrine based Schiff bases. Spectrochimica Acta Part A: Molecular and Biomolecular Spectroscopy. 2020;233:118231.
22. Tercan M, Özdemir N, Özdemir FA, Şerbetçi Z, Erdener D, Çetinkaya B, et al. Synthesis, DFT computations and antimicrobial activity of a Schiff base derived from 2-hydroxynaphthaldehyde: Remarkable solvent effect. Journal of Molecular Structure. 2020;1209:127980.
23. Sumrra SH, Sahrish I, Raza MA, Ahmad Z, Zafar MN, Chohan ZH, et al. Efficient synthesis, characterization, and in vitro bactericidal studies of unsymmetrically substituted triazole-derived Schiff base ligand and its transition metal complexes. Monatshefte für Chemie - Chemical Monthly. 2020;151(4):549-557.
24. Abu-Dief AM, El-khatib RM, Aljohani FS, Alzahrani SO, Mahran A, Khalifa ME, et al. Synthesis and intensive characterization for novel Zn(II), Pd(II), Cr(III) and VO(II)-Schiff base complexes; DNA-interaction, DFT, drug-likeness and molecular docking studies. Journal of Molecular Structure. 2021;1242:130693.
25. Synthesis and Characterization of New Schiff Base Ligand Derived from 4- aminoantipyrine and its complexes with some metal ions and Their Fluorescence Study. International Journal of Pharmaceutical Research. 2020;13(01).
26. Alkhatib F, Hameed A, Sayqal A, Bayazeed AA, Alzahrani S, Al-Ahmed ZA, et al. Green-synthesis and characterization for new Schiff-base complexes; spectroscopy, conductometry, Hirshfeld properties and biological assay enhanced by in-silico study. Arabian Journal of Chemistry. 2020;13(8):6327-6340.
27. Alharbi A, Alzahrani S, Alkhatib F, Abu Al-Ola K, Abdulaziz Alfi A, Zaky R, et al. Studies on new Schiff base complexes synthesized from d10 metal ions: Spectral, conductometric measurements, DFT and docking simulation. J Mol Liq. 2021;334:116148.
28. Saritha TJ, Metilda P. Synthesis, spectroscopic characterization and biological applications of some novel Schiff base transition metal (II) complexes derived from curcumin moiety. Journal of Saudi Chemical Society. 2021;25(6):101245.
29. Sakthivel RV, Sankudevan P, Vennila P, Venkatesh G, Kaya S, Serdaroğlu G. Experimental and theoretical analysis of molecular structure, vibrational spectra and biological properties of the new Co(II), Ni(II) and Cu(II) Schiff base metal complexes. Journal of Molecular Structure. 2021;1233:130097.
30. Kareem MJ, Al-Hamdani AAS, Jirjees VY, Khan ME, Allaf AW, Al Zoubi W. Preparation, spectroscopic study of Schiff base derived from dopamine and metal Ni(II), Pd(II), and Pt(IV) complexes, and activity determination as antioxidants. J Phys Org Chem. 2020;34(3).
31. Buldurun K, Turan N, Çolak N, Özdemir İ. Schiff Base and

Its Fe(II), Zn(II), Ru(II), Pd(II) Complexes Containing ONS Donor Atoms: Synthesis, characterization and Catalytic Studies. Deu Muhendislik Fakultesi Fen ve Muhendislik. 2019;21(61):73-82.
32. Sundararajan ML, Jeyakumar T, Anandakumaran J, Karpanai Selvan B. Synthesis of metal complexes involving Schiff base ligand with methylenedioxy moiety: Spectral, thermal, XRD and antimicrobial studies. Spectrochimica Acta Part A: Molecular and Biomolecular Spectroscopy. 2014;131:82-93.
33. Buldurun K, Turan N, Bursal E, Aras A, Mantarcı A, Çolak N, et al. Synthesis, characterization, powder X-ray diffraction analysis, thermal stability, antioxidant properties and enzyme inhibitions of M(II)-Schiff base ligand complexes. Journal of Biomolecular Structure and Dynamics. 2020;39(17):6480-6487.
34. Abdel Aziz AA, Seda SH. Synthesis, Spectral Characterization, SEM, Antimicrobial, Antioxidative Activity Evaluation, DNA Binding and DNA Cleavage Investigation of Transition Metal(II) Complexes Derived from a tetradentate Schiff base bearing thiophene moiety. Journal of Fluorescence. 2017;27(3):1051-1066.
35. de Araújo EL, Barbosa HFG, Dockal ER, Cavalheiro ÉTG. Synthesis, characterization and biological activity of Cu(II), Ni(II) and Zn(II) complexes of biopolymeric Schiff bases of salicylaldehydes and chitosan. Int J Biol Macromol. 2017;95:168-176.
36. Mawat TH, Al-Jeboori MJ. Synthesis, characterisation, thermal properties and biological activity of coordination compounds of novel selenosemicarbazone ligands. Journal of Molecular Structure. 2020;1208:127876.
37. Wang Y-P, Jiang T-T, Wang Y-C, Dong H-X, Lu J, Jin J, et al. Synthesis, crystal structure, spectral characterization and antimicrobial activity of Zn(II) and Ni(II) compounds with the Schiff base ligand 3, 5-dichlorosalicylaldehyde o-phenylenediamine. Journal of Molecular Structure. 2024;1301:137450.
38. Salomanravi A, Muthuselvan P, Paularokiadoss F, Christopher Jeyakumar T. Synthesis, structure, DNA/BSA binding, antibacterial and molecular docking studies of tetradentate ONNO schiff base metal complexes. Journal of Molecular Structure. 2023;1287:135570.
39. Kyhoiesh HAK, Al-Adilee KJ. Pt(IV) and Au(III) complexes with tridentate-benzothiazole based ligand: synthesis, characterization, biological applications (antibacterial, antifungal, antioxidant, anticancer and molecular docking) and DFT calculation. Inorg Chim Acta. 2023;555:121598.
40. Al-Janabi ASM, Oudah KH, Aldossari SA, Khalaf MA, M. Saleh A, Hatshan MR, et al. Spectroscopic, anti-bacterial, anti-cancer and molecular docking of Pd(II) and Pt(II) complexes with (E)-4-((dimethylamino)methyl)-2-((4,5-dimethylthiazol-2-yl)diazenyl)phenol ligand. Journal of Saudi Chemical Society. 2023;27(3):101619.
41. Al-Adilee KJ, Atyha SA. Synthesis, Spectral, Thermal and Biological Studies of Some Metal Complexes Derived from Heterocyclic Mono Azo Dye Ligand 2'[(2'-Hydroxy-4-methyl phenyl)azo]imidazole. Asian J Chem. 2018;30(2):280-292.